J Mater Sci (2006) 41:6991–7004
DOI 10.1007/s10853-006-0232-3

Modeling bamboo as a functionally graded material: lessons for the analysis of affordable materials

Emílio Carlos Nelli Silva · Matthew C. Walters · Glaucio H. Paulino

Published online: 16 September 2006

Abstract Natural fibers are promising for engineering applications due to their low cost. They are abundantly available in tropical and subtropical regions of the world, and they can be employed as construction materials. Among natural fibers, bamboo has been widely used for housing construction around the world. Bamboo is an optimized composite that exploits the concept of Functionally Graded Material (FGM). Biological structures such as bamboo have complicated microstructural shapes and material distribution, and thus the use of numerical methods such as the finite element method, and multiscale methods such as homogenization, can help to further understanding of the mechanical behavior of these materials. The objective of this work is to explore techniques such as the finite element method and homogenization to investigate the structural behavior of bamboo. The finite element formulation uses graded finite elements to capture the varying material distribution through the bamboo wall. To observe bamboo behavior under applied loads, simulations are conducted under multiple considerations such as a spatially varying Young's modulus, an averaged Young's modulus, and orthotropic constitutive properties obtained from homogenization theory. The homogenization procedure uses effective, axisymmetric properties estimated from the spatially varying bamboo composite. Three-dimensional models of bamboo cells were built and simulated under tension, torsion, and bending load cases.

E. C. N. Silva
Department of Mechatronics and Mechanical Systems Engineering, Escola Politécnica da Universidade de São Paulo, Av. Professor Mello Moraes, 2231, São Paulo, SP 05508-900, Brazil

M. C. Walters · G. H. Paulino (✉)
Department of Civil and Environmental Engineering, University of Illinois at Urbana-Champaign, Newmark Laboratory, 205 North Mathews Avenue, Urbana, IL 61801, USA
e-mail: paulino@uiuc.edu

Introduction

Biological systems such as plant and tree stems, animal bones and other biological hard tissues tend to be optimized for the loading conditions they are subjected to. Their geometry changes with loading conditions to match stress- or strain-dependent requirements, and their material properties are also optimally distributed. For example, the interior structure of bone changes depending on the principal stress directions and the magnitude of shear stress they carry [1].

Biological structures are usually made of composite materials which are multifunctional and have living organisms which provides adaptability. This occurs due to the fact that biological systems must be able to perform a variety of functions well, and thus, they are optimized for multifunctional purposes. As a consequence, biological structures are complicated and non-uniform, which makes their realistic modeling difficult and involved.

Among biological structures, the natural fibers are very interesting for engineering applications due to their low cost and convenient availability. They grow abundantly in tropical and subtropical regions of the world, and they can be usefully employed as con-

struction materials [2–4]. Examples of natural fibers are bamboo, coconut fibers, sisal, etc. Among the natural fibers, bamboo finds widespread use in housing construction around the world, and is considered as a promising housing material in underdeveloped and developed countries. Recently, some studies investigating composites made of bamboo and concrete [5] and bamboo and polymer [6, 7] have been conducted.

Bamboo is a tree-like plant (see Fig. 1(a)) that belongs to the subfamily *Bambusoideae* of the grass family *Poaceae*. Bamboo stalks are optimized composite materials that naturally exploit the concept of Functionally Graded Materials (FGMs) [1, 9–13]. Such materials possess continuously graded properties and are characterized by spatially varying microstructures created by non-uniform distributions of the constituent phases. In these materials, the role of reinforcement and matrix (base) material interchanges in a continuous manner [14]. The smooth variation of properties may offer advantages such as reduction of stress concentration and increased bonding strength [15, 16].

The bamboo culm is an approximately cylindrical shell that is divided periodically by transversal diaphragms at nodes. Between 20% and 30% of the cross-sectional area of the culm is made of longitudinal fibers that are distributed non-uniformly through the wall thickness, the concentration being most dense near the exterior (see Fig. 1(b)). The orientation of these fibers makes bamboo an orthotropic material with high strength along, and low strength transversal to fibers [5, 17, 18].

Most work in the literature that characterizes bamboo is experimental, dedicated to estimating strength and stiffness properties [17–23]. Few works treating the modeling of natural fibers have been found in the literature [24, 25], and these deal primarily with simplified analytical models. In these studies, comprehensive experimental characterization of certain species of bamboo were performed by measuring strength, Young's modulus of matrix and fiber, and through analysis of microstructures and fiber distribution [1, 9, 10, 25]. Bamboo exhibits a piezoelectric effect, also existing in bone, that helps the bamboo to control the modeling/remodeling of its microstructure based on external mechanical stimuli. This behavior makes it a self-optimizing system with natural sensing mechanisms [1].

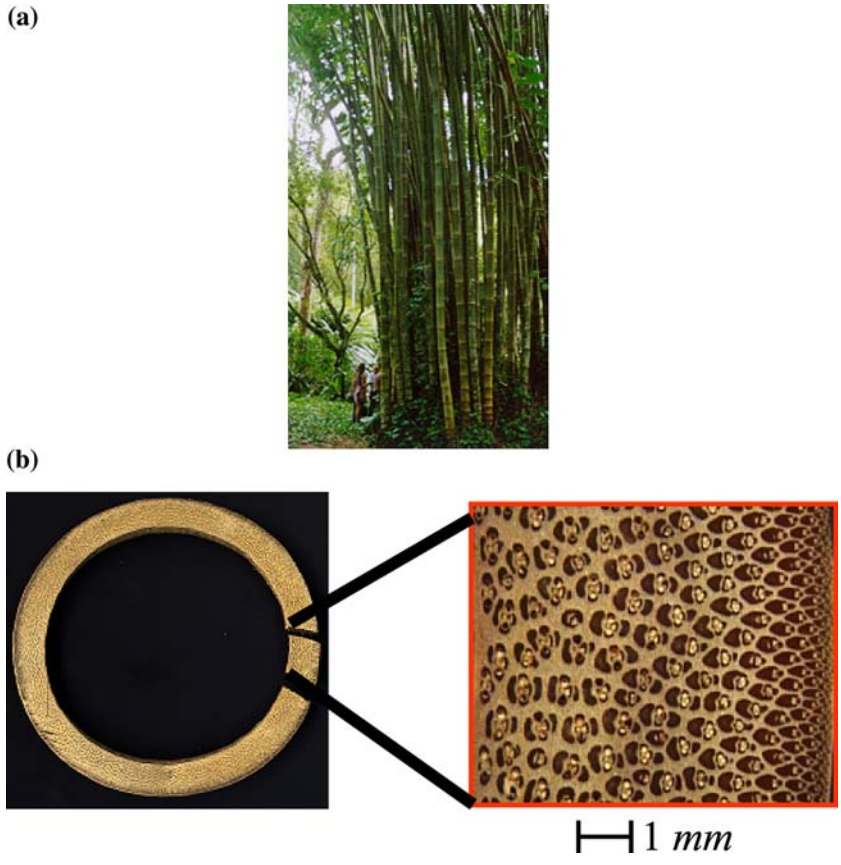

Fig. 1 (**a**) Bamboo stalks; (**b**) Cross section of culm showing radial distribution of fibers through the thickness (photo courtesy of [8])

Nogata and Takahashi [1] have provided an analytical model for bamboo mechanical behavior based on composite beam theory. Another analytical model based on the solution of the Laplace equation has been applied by Amada and Terauchi [24] to find the maximum shear stress in the triangular section of a hemp palm tree when subjected to torsional loads. Hemp palm and bamboo have a very similar structural behavior, as both have a dense distribution of fibers near the exterior of the stem.

Considering that biological structures, such as bamboo, have complicated shapes and material distribution inside their domain, the use of numerical methods such as the finite element method (FEM) [26, 27] can be a useful tool for understanding the mechanical behavior of these materials. Also, since natural fibers in general make a composite material with an identifiable microstructure, multiscale methods, such as homogenization [28], can be applied to estimate how the microstructure influences the effective properties of these materials. The objective of this work is to explore computational techniques including the FEM and a multi-scale method based on homogenization, to investigate the structural behavior of bamboo. First, the finite element formulation employed herein uses the so-called graded finite elements (e.g., [29, 30]) which capture the influence of spatially varying material properties by means of a generalized isoparametric formulation (GIF). The traditional FEM approach approximates material gradation using constant properties in each element, leading to a less accurate simulation of FGM behavior. Second, the multi-scale method employed here is based on the homogenization method, which enables the computation of effective properties of a composite material. With these properties, it is possible to model the composite structure as an equivalent homogeneous medium, allowing the use of traditional FEM codes or simple analytical models for numerical modeling. A third set of simulations employs a homogeneous, averaged value of Young's modulus, allowing comparisons and demonstrating the limitations of simplified procedures.

The remainder of this study is organized as follows. In Section 2, the theoretical formulation of graded finite elements is briefly described. In Section 3, the homogenization theory for axisymmetric FGM composite materials is developed. In Section 4, some representative results from tension, torsion and bending analyses are presented to illustrate the difference between the numerical approaches, and to observe the mechanical behavior of bamboo. Finally, in Section 5, concluding remarks complete the present work.

Modeling bamboo with graded finite elements

When modeling a functionally graded material using the FEM, the continuous variation of material properties within the domain must be accounted for. In the traditional finite element formulation [26], the properties are assumed to be constant inside each element. To model an FGM using this traditional formulation, a continuous material distribution is approximated by piecewise-constant elements. This generates an artificially discontinuous stress field, however, which may not adequately simulate the actual conditions. An FEM formulation better-suited for FGMs employs graded elements that incorporate actual material properties at integration points [30]. For graded elements, the element stiffness matrix, $\mathbf{k}^e$, is given by (e.g., [26, 27])

$$\mathbf{k}^e = \int_{\Omega_e} (\mathbf{B}^e)^T \mathbf{E}^e(\mathbf{x}) \mathbf{B}^e d\Omega_e, \tag{1}$$

in which Ω_e is the domain of element e, $\mathbf{B}^e$ is the element strain-displacement matrix, $\mathbf{E}^e(\mathbf{x})$ is the matrix of constitutive properties and T denotes the matrix transpose. The spatial coordinate $\mathbf{x} = (x, y)$ is interpolated using finite-element nodal shape functions, N_I, corresponding to element node I:

$$x = \sum_{I=1}^{m} N_I x_I, \quad y = \sum_{I=1}^{m} N_I y_I, \tag{2}$$

where m is the number of element nodes. Thus, if the material variation is known, Eq. (1) can be evaluated numerically at each integration point using values of $E(x,y)$ and $v(x,y)$ in $\mathbf{E}^e(\mathbf{x})$. Evaluation of material properties at integration points in a finite element is illustrated in Fig. 2. Gaussian integration of Eq. (1) in parent coordinates ξ and η for a two-dimensional (2-D) element is thus expressed as:

$$\begin{aligned} \mathbf{k}^e &= \int_{-1}^{1}\int_{-1}^{1} (\mathbf{B}^e)^T \mathbf{E}^e(\xi,\eta) \mathbf{B}^e \det J d\xi d\eta \\ &\cong \sum_{i=1}^{ng}\sum_{j=1}^{ng} w_i w_j \left(\mathbf{B}^e\left(\xi_i,\eta_j\right)\right)^T \mathbf{E}^e\left(\xi_i,\eta_j\right) \mathbf{B}^e\left(\xi_i,\eta_j\right) \\ &\quad \det J\left(\xi_i,\eta_j\right), \end{aligned} \tag{3}$$

where ng is the number of Gaussian integration points in each parent coordinate, w_i is the weight corresponding to integration point i, and det J is the determinant of the coordinate Jacobian. This procedure using graded elements incorporates continuous material distribution into the numerical simulation,

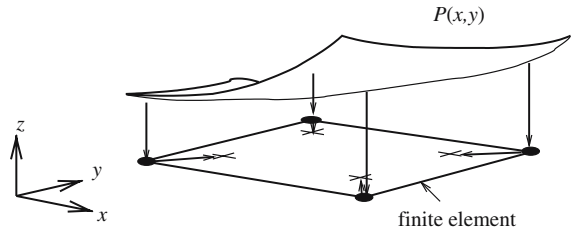

Fig. 2 Determination of material properties $P(x,y)$ at integration points of a graded finite element (generalized isoparametric formulation, or GIF [30])

and leads to smoothly varying and more accurate stresses [30].

Homogenization theory for functionally graded axisymmetric composites

The combination of two or more materials in a composite ideally leads to substantial advantages in performance over that offered by individual constituents. By altering the volume fraction of the constituents, the shape of inclusions, or even the topology of the periodic microstructure, it is possible to obtain different effective properties for the composite material. A periodic composite material is a composite whose microstructure exhibits a periodic repetition of a representative substructure called a unit cell [31, 32]. A recent micromechanics model considering the effects of particle interaction and material gradients has been presented by Yin et al. [33].

The homogenization method enables the estimation of effective properties of a complex periodic composite material with a known unit-cell topology. It is a general method for computing effective properties and has no limitations regarding volume fraction or shape of the composite constituents. The primary assumptions are that the unit cell is periodic and that the scale of the composite part is much larger than the microstructure dimensions [28, 34]. An important consideration that arises when computing effective properties of composite materials is the effect of the specimen scale with respect to the scale of the unit cell. A direct approach to obtain the effective properties of a composite material is to subject a specimen to simple loads such as tension, compression, torsion, and then estimate the effective properties from measured or imposed displacements [33]. This process can be performed either experimentally or using numerical (e.g., FEM) simulations [31]. However, if the specimen size is not large enough in relation to the unit cell dimensions, the estimated properties will be influenced by ''size effect.'' That is, the boundary conditions of the specimen will interfere with the behavior of the unit cell, and the measured or computed properties will be subsequently affected. Homogenization theory, as developed in this work, eliminates this problem by decoupling the unit cell behavior from the specimen behavior. Bamboo can be considered an axisymmetric composite material. Thus, homogenization theory for axisymmetric composite materials will be described.

Theoretical formulation

An axisymmetric composite and its corresponding 2-D unit cell is illustrated in Fig. 3. Considering the standard homogenization procedure for elastic materials [34], the unit cell is defined as $\mathbf{Y} = [0, Y_1] \times [0, Y_2]$ and the elastic property function E_{ijkl} is considered to be a Y-periodic function:

$$\mathbf{E}^{\varepsilon}(\mathbf{x}) = \mathbf{E}(\mathbf{x},\mathbf{y}) = \begin{bmatrix} E_{11}(\mathbf{x},\mathbf{y}) & E_{12}(\mathbf{x},\mathbf{y}) & E_{13}(\mathbf{x},\mathbf{y}) & 0 \\ E_{12}(\mathbf{x},\mathbf{y}) & E_{22}(\mathbf{x},\mathbf{y}) & E_{23}(\mathbf{x},\mathbf{y}) & 0 \\ E_{13}(\mathbf{x},\mathbf{y}) & E_{23}(\mathbf{x},\mathbf{y}) & E_{33}(\mathbf{x},\mathbf{y}) & 0 \\ 0 & 0 & 0 & E_{44}(\mathbf{x},\mathbf{y}) \end{bmatrix}; \tag{4}$$

$$\mathbf{E}^{\varepsilon}(\mathbf{x},\mathbf{y}) = \mathbf{E}(\mathbf{x},\mathbf{y}+\mathbf{Y}), \text{ and } \mathbf{y} = \mathbf{x}/\varepsilon, \tag{5}$$

where $\varepsilon > 0$ is the composite microstructure scale that represents the scale in which the material properties are changing. Coordinates $\mathbf{x} = (r, z)$ and $\mathbf{y} = (s, w)$ are associated with the composite macro- and micro-dimensions, respectively (see Fig. 3). The first step in the homogenization procedure is to expand the displacement $\mathbf{u}$ inside the unit cell as [28]

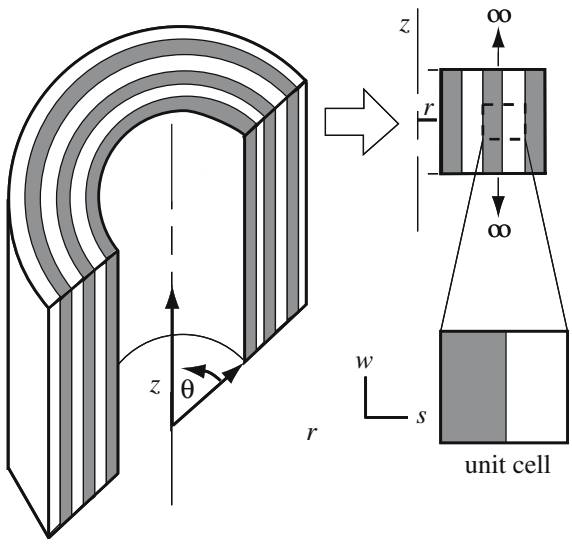

Fig. 3 An axisymmetric composite and its corresponding unit cell

$$\mathbf{u}^{\varepsilon} = \left\{ u_r^{\varepsilon} \quad u_z^{\varepsilon} \right\}^T = \mathbf{u}_0(\mathbf{x}) + \varepsilon \mathbf{u}_1(\mathbf{x}, \mathbf{y}), \tag{6}$$

where only the first-order variation terms ($\mathbf{u}_1(\mathbf{x}, \mathbf{y})$) are taken into account, and $\mathbf{u}_1$ is Y-periodic. Displacements $\mathbf{u}_0(\mathbf{x})$ and $\mathbf{u}_1(\mathbf{x}, \mathbf{y})$ correspond to the composite specimen scale and the unit cell scales, respectively [28, 34]. Notice that $\mathbf{u}_0(\mathbf{x})$ depends only on the composite specimen (macro) coordinates $\mathbf{x}$, and $\mathbf{u}_1(\mathbf{x}, \mathbf{y})$ depends on the macro coordinates and the unit cell (micro) coordinates $\mathbf{y}$. When bamboo is subjected to axisymmetric loading, it can be modeled as a fully axisymmetric composite. In this study, we will use this assumption, and therefore employ cylindrical coordinates. The strain is then written as [26]

$$\begin{aligned}
\varepsilon^{\varepsilon} &= \partial_x \mathbf{u}^{\varepsilon} = \left\{ \frac{\partial u_r^{\varepsilon}}{\partial r} \quad \frac{u_r^{\varepsilon}}{r} \quad \frac{\partial u_z^{\varepsilon}}{\partial z} \quad \frac{\partial u_z^{\varepsilon}}{\partial r} + \frac{\partial u_r^{\varepsilon}}{\partial z} \right\}^T \\
&= \partial_x \mathbf{u}_0(\mathbf{x}) + \varepsilon \partial_x \mathbf{u}_1(\mathbf{x}, \mathbf{y}) + \partial_y \mathbf{u}_1(\mathbf{x}, \mathbf{y}) \\
&= \left\{ \frac{\partial u_r^0}{\partial r} \quad \frac{u_r^0}{r} \quad \frac{\partial u_z^0}{\partial z} \quad \frac{\partial u_z^0}{\partial r} + \frac{\partial u_r^0}{\partial z} \right\}^T \\
&+ \varepsilon \left\{ \frac{\partial u_r^1}{\partial r} \quad \frac{u_r^1}{r} \quad \frac{\partial u_z^1}{\partial z} \quad \frac{\partial u_z^1}{\partial r} + \frac{\partial u_r^1}{\partial z} \right\}^T \\
&+ \left\{ \frac{\partial u_r^1}{\partial s} \quad 0 \quad \frac{\partial u_z^1}{\partial w} \quad \frac{\partial u_z^1}{\partial s} + \frac{\partial u_r^1}{\partial w} \right\}^T,
\end{aligned} \tag{7}$$

where the chain rule was applied for the $\partial_y \mathbf{u}_1(\mathbf{x}, \mathbf{y})$ term. Equations (6) and (7), and properties described by (5) must be substituted into the energy functional for the elastic medium, and the variation of this functional taken with respect to $\mathbf{u}^{\varepsilon}$. Passing to the limit $\varepsilon \to 0$, one obtains [28]

$$\lim_{\varepsilon \to 0} \int_{\Omega} \Phi\left(\mathbf{x}, \frac{\mathbf{x}}{\varepsilon}\right) d\Omega = \frac{1}{|Y|} \int_{\Omega} \int_{Y} \Phi\left(\mathbf{x}, \frac{\mathbf{x}}{\varepsilon}\right) dY d\Omega, \tag{8}$$

where $\Phi\left(\mathbf{x}, \frac{\mathbf{x}}{\varepsilon}\right)$ represents an arbitrary function. After taking the limit $\varepsilon \to 0$, only the terms $\partial_x \mathbf{u}_0(\mathbf{x})$ (and $\delta \mathbf{u}_0(\mathbf{x})$) and $\partial_y \mathbf{u}_1(\mathbf{x}, \mathbf{y})$ (and $\delta \mathbf{u}_1(\mathbf{x}, \mathbf{y})$) will be present in the equations. The term $\partial_x \mathbf{u}_0(\mathbf{x})$ (and $\delta \mathbf{u}_0(\mathbf{x})$) denotes the overall strain in the composite specimen, and the term $\partial_y \mathbf{u}_1(\mathbf{x}, \mathbf{y})$ (and $\delta \mathbf{u}_1(\mathbf{x}, \mathbf{y})$) denotes the unit cell strain. Notice that from Eq. (7), the strain $\partial_y \mathbf{u}_1(\mathbf{x}, \mathbf{y})$ (and $\delta \mathbf{u}_1(\mathbf{x}, \mathbf{y})$) does not have a hoop strain term, which means that the unit cell behavior can be treated simply as a plane-strain behavior. This is reasonable because the unit cell behavior should be defined only by the microscale. In addition, notice that Eq. (8) separates the integration over the unit cell domain and the composite specimen domain. This means that we do not need to perform the integration in a coordinate system that coincides with that used to define the composite body (e.g., cylindrical). Since the unit cell has a plane strain behavior, it is more convenient to define $\mathbf{y}$ in a cartesian coordinate system, as illustrated in Fig. 3.

By considering the terms involving $\delta \mathbf{u}_1(\mathbf{x}, \mathbf{y})$ and $\delta \mathbf{u}_0(\mathbf{x})$, we obtain distinct microscopic and macroscopic equations, respectively. Due to the linearity of the problem, and assuming the separation of variables for $\mathbf{u}_1(\mathbf{x}, \mathbf{y})$, we obtain [28]:

$$\begin{aligned}
\mathbf{u}_1 = \begin{Bmatrix} u_r^1 \\ u_z^1 \end{Bmatrix} = \chi(\mathbf{x}, \mathbf{y}) \varepsilon(\mathbf{u}_0(\mathbf{x})) = &\begin{Bmatrix} \chi_r^{11} & \chi_z^{11} \\ \chi_r^{22} & \chi_z^{22} \\ \chi_r^{33} & \chi_z^{33} \\ \chi_r^{44} & \chi_z^{44} \end{Bmatrix}^T \\
&\begin{Bmatrix} \frac{\partial u_r^0}{\partial r} \\ \frac{u_r^0}{r} \\ \frac{\partial u_z^0}{\partial z} \\ \frac{\partial u_z^0}{\partial r} + \frac{\partial u_r^0}{\partial z} \end{Bmatrix},
\end{aligned} \tag{9}$$

and

$$\begin{aligned}
\partial_y \mathbf{u}_1(\mathbf{x}, \mathbf{y}) &= \left\{ \frac{\partial u_r^1}{\partial s} \quad 0 \quad \frac{\partial u_z^1}{\partial w} \quad \frac{\partial u_z^1}{\partial s} + \frac{\partial u_r^1}{\partial w} \right\}^T \\
&= \partial_y \chi(\mathbf{x}, \mathbf{y}) \partial_x (\mathbf{u}_0(\mathbf{x})) \\
&= \begin{Bmatrix} \frac{\partial \chi_r^{11}}{\partial s} & 0 & \frac{\partial \chi_z^{11}}{\partial w} & \frac{\partial \chi_z^{11}}{\partial s} + \frac{\partial \chi_r^{11}}{\partial w} \\ \frac{\partial \chi_r^{22}}{\partial s} & 0 & \frac{\partial \chi_z^{22}}{\partial w} & \frac{\partial \chi_z^{22}}{\partial s} + \frac{\partial \chi_r^{22}}{\partial w} \\ \frac{\partial \chi_r^{33}}{\partial s} & 0 & \frac{\partial \chi_z^{33}}{\partial w} & \frac{\partial \chi_z^{33}}{\partial s} + \frac{\partial \chi_r^{33}}{\partial w} \\ \frac{\partial \chi_r^{44}}{\partial s} & 0 & \frac{\partial \chi_z^{44}}{\partial w} & \frac{\partial \chi_z^{44}}{\partial s} + \frac{\partial \chi_r^{44}}{\partial w} \end{Bmatrix}^T \begin{Bmatrix} \frac{\partial u_r^0}{\partial r} \\ \frac{u_r^0}{r} \\ \frac{\partial u_z^0}{\partial z} \\ \frac{\partial u_z^0}{\partial r} + \frac{\partial u_r^0}{\partial z} \end{Bmatrix},
\end{aligned} \tag{10}$$

where $\chi(\mathbf{x}, \mathbf{y})$ is the characteristic displacement of the unit cell, which is also Y-periodic, belonging to $H_{\text{per}}(Y, R^3)$:

$$\begin{aligned}
H_{\text{per}}(Y, R^3) &= \left\{ \mathbf{v} = (v_i) | v_i \in H_{\text{per}}(Y), i = 1, 2, 3 \right\} \\
H_{per}(Y) &= \{ v \in H^1(Y) | v \text{ takes equal values} \\
&\qquad \text{on opposite sides of } Y. \},
\end{aligned} \tag{11}$$

which corresponds to the periodicity condition in the unit cell, as illustrated in Fig. 4. Then, substituting Eq. (10) into the unit-cell (microscopic) equations, we obtain [34]

$$\begin{aligned}
&\frac{1}{|Y|} \int_Y \left[\left(\mathbf{I} + \partial_y \chi(\mathbf{x}, \mathbf{y}) \right) : \mathbf{E}(\mathbf{x}, \mathbf{y}) : \partial_y \delta \mathbf{u}_1(\mathbf{x}, \mathbf{y}) \right] dY = 0, \\
&\quad \forall \delta \mathbf{u}_1 \in H_{\text{per}}(Y, R^3),
\end{aligned} \tag{12}$$

or in index notation:

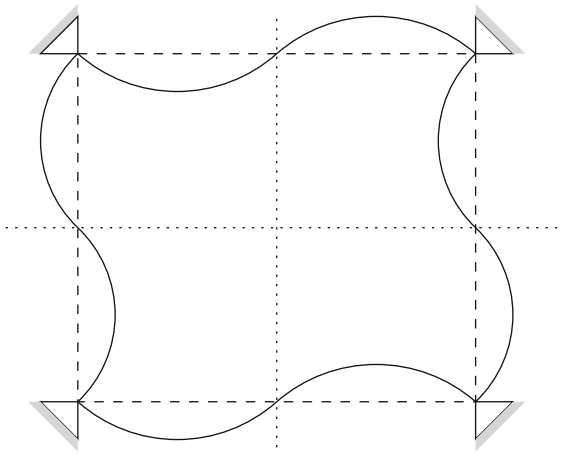

Fig. 4 Illustration of periodicity conditions in the unit cell

$$\frac{1}{|Y|}\int_Y E_{ijkl}(\mathbf{x},\mathbf{y})\left(\delta_{im}\delta_{jn}+\frac{\partial\chi_i^{(mn)}}{\partial y_j}\right)\varepsilon_{kl}(\mathbf{v})dY=0, \quad \forall\mathbf{v}\in H_{\text{per}}(Y,R^3). \tag{13}$$

Substituting Eq. (10) into the specimen (macroscopic) equations, the definition of the effective properties can be obtained [34]:

$$\mathbf{E}^H=\frac{1}{|Y|}\int_Y\left[\mathbf{E}(\mathbf{x},\mathbf{y}):\left(\mathbf{I}+\partial_y\chi(\mathbf{x},\mathbf{y})\right)\right]dY. \tag{14}$$

By using Eq. (12), Eq. (14) becomes

$$\mathbf{E}^H=\frac{1}{|Y|}\int_Y[(\mathbf{I}+\partial_y\chi(\mathbf{x},\mathbf{y})):\mathbf{E}(\mathbf{x},\mathbf{y}):(\mathbf{I}+\partial_y\chi(\mathbf{x},\mathbf{y}))]dY, \tag{15}$$

or in index notation:

$$E^H_{rspq}(\mathbf{x})=\frac{1}{|Y|}\int_Y E_{ijkl}(\mathbf{x},\mathbf{y})\left(\delta_{ip}\delta_{jq}+\frac{\partial\chi_i^{(pq)}}{\partial y_j}\right)\left(\delta_{kr}\delta_{ls}+\frac{\partial\chi_k^{(rs)}}{\partial y_l}\right)dY, \tag{16}$$

where $E^H_{ijkl}=E^H_{klij}=E^H_{jikl}$. Notice that due to the plane-strain behavior of the unit cell, (that is, the term $\partial_y\mathbf{u}_1(\mathbf{x},\mathbf{y})$ has a null hoop strain term), the homogenized elasticity coefficients E^H_{12} and E^H_{22} will be an average of the coefficients E_{12} and E_{22} inside the unit cell domain. Thus, we are able to compute the effective properties of an axisymmetric composite material such as a bamboo.

Numerical implementation

This section presents the numerical implementation of the above homogenization procedure, and incorporates the influence of spatially varying material properties. The expressions in Eq. (13) are evaluated using FEM, with a unit cell discretized by N finite elements. Thus

$$Y=\cup_{n=1}^N\Omega^e, \tag{17}$$

where Ω^e is the domain of each element. Four-noded elements with two displacement degrees of freedom per node and bilinear interpolation functions were used in the mesh [26]. The characteristic functions previously defined are interpolated within each element using standard shape functions (N_I):

$$\chi_i^{(mn)}\cong\sum_{I=1}^{nodes}N_I\chi_{iI}^{(mn)}, \tag{18}$$

where nodes is the number of *nodes* per finite element (for example, four in the 2-D case). Similar relations hold for the virtual displacement $\mathbf{v}$. Substituting Eq. (18) into Eq. (12), and assembling the individual matrices for each element, we obtain the following global matrix system for each load case mn or m [34]:

$$[\mathbf{K_{uu}}]\left\{\widehat{\chi}^{(mn)}\right\}=\left\{\mathbf{F}^{(mn)}\right\}, \tag{19}$$

where $\widehat{\chi}$ are the corresponding nodal values of the characteristic function χ. The global stiffness is the assembly (denoted by A_e) of each element's individual matrix, and the global force $\mathbf{F}$ is the assembly of the individual force vectors for all elements, i.e.,

$$\mathbf{K_{uu}}=A_{e=1}^N\mathbf{K}^e_{\mathbf{uu}},\quad \mathbf{F}=A_{e=1}^N\mathbf{F}^e. \tag{20}$$

The element matrices and vectors are given by the expressions [34]:

$$K^e_{uu(iIjJ)}=\int_{\Omega^e}E_{ipjq}\frac{\partial N_I}{\partial y_p}\frac{\partial N_I}{\partial y_q}d\Omega^e\quad F_{iI}^{e(mn)}=\int_{\Omega^e}E_{ijmn}\frac{\partial N_I}{\partial y_j}d\Omega^e. \tag{21}$$

Thus, for the 2-D problem, there are three load cases to be solved independently, as illustrated in Fig. 5. They come from Eq. (19), where the indices mn can assume the values 11, 33, or 44. All load cases must be solved by enforcing periodic displacement boundary conditions in the unit cell (see Fig. 4). The unit cell problem is solved in $\mathbf{y}$ cartesian coordinates assuming plane-strain conditions. In addition, because the domain of the unit cell comprises graded material, as illustrated in Fig. 6, material property terms must remain in the integrand during the Gauss quadrature. Integration of order 2 in each direction (2×2 rule) is

applied here to evaluate the integrals in Eqs. (15) and (21) which yield the effective properties. The displacements of some node in the unit cell mesh must be prescribed in order to avoid the non-uniqueness of the problem solution. Without this condition, the FEM problem is ill-posed. When computing the effective properties through Eq. (15) assuming axisymmetry, the hoop strain term in $\partial_y \chi(\mathbf{x}, \mathbf{y})$ is set to zero.

Example computations of effective bamboo properties

To illustrate the homogenization technique, we consider a fictitious axisymmetric, isotropic composite composed of two basic materials, as illustrated in Figs. 3 and 6. Accordingly, on the normalized variable s: let the material variation for the unit cell in this example be approximated by the periodic expression

$$\mathbf{E}(s) = [(\mathbf{E}_1 - \mathbf{E}_2)\cos 2\pi s + \mathbf{E}_1 + \mathbf{E}_2]/2, \tag{22}$$

where s is the normalized coordinate defined in Fig. 6, and $\mathbf{E}_1$ and $\mathbf{E}_2$ are the axisymmetric stiffness tensors for the two materials. The material stiffness tensors have components expressed as:

$$\mathbf{E}_i = \frac{(1-v_i)E_i}{(1+v_i)(1-2v_i)} \begin{bmatrix} 1 & \frac{v_i}{1-v_i} & \frac{v_i}{1-v_i} & 0 \\ \frac{v_i}{1-v_i} & 1 & \frac{v_i}{1-v_i} & 0 \\ \frac{v_i}{1-v_i} & \frac{v_i}{1-v_i} & 1 & 0 \\ 0 & 0 & 0 & \frac{1-2v_i}{2(1-v_i)} \end{bmatrix}. \tag{23}$$

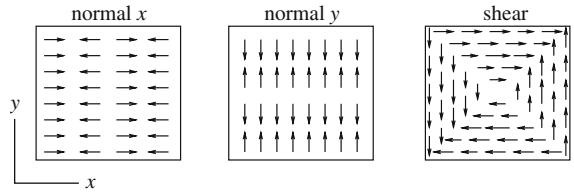

Fig. 5 Basic load cases applied to the unit cell

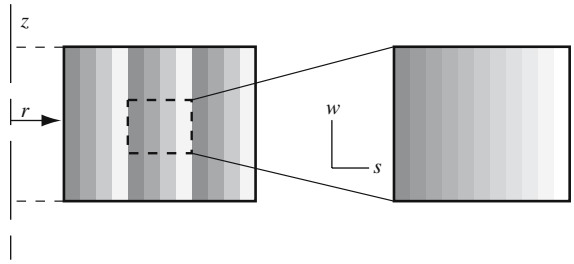

Fig. 6 Axisymmetric FGM composite and its corresponding unit cell with a continuous material gradation

If, for example, E_1=55 GPa, E_2=2 GPa, and Poisson's ratio v=0.35, then $\mathbf{E}_1$ and $\mathbf{E}_2$ are:

$$\begin{aligned} \mathbf{E}_1 &= \begin{bmatrix} 88.27 & 47.53 & 47.53 & 0 \\ 47.53 & 88.27 & 47.53 & 0 \\ 47.53 & 47.53 & 88.27 & 0 \\ 0 & 0 & 0 & 9.81 \end{bmatrix} \text{GPa}, \\ \mathbf{E}_2 &= \begin{bmatrix} 3.21 & 1.73 & 1.73 & 0 \\ 1.73 & 3.21 & 1.73 & 0 \\ 1.73 & 1.73 & 3.21 & 0 \\ 0 & 0 & 0 & 0.36 \end{bmatrix} \text{GPa}. \end{aligned} \tag{24}$$

In this case the effective orthotropic axisymmetric elasticity tensor, computed through the homogenization procedure described above using a 20×20 mesh of Q4 elements for the unit cell, is:

$$\mathbf{E}^H = \begin{bmatrix} 15.95 & 6.83 & 6.83 & 0 \\ 6.83 & 38.37 & 12.32 & 0 \\ 6.83 & 12.32 & 34.25 & 0 \\ 0 & 0 & 0 & 4.56 \end{bmatrix} \text{GPa}. \tag{25}$$

The axisymmetric stress-strain relation is then expressed as

$$\{\, \sigma_{rr} \quad \sigma_{\theta\theta} \quad \sigma_{zz} \quad \tau_{rz} \,\}^T = \mathbf{E}^H \{\, \varepsilon_{rr} \quad \varepsilon_{\theta\theta} \quad \varepsilon_{zz} \quad \gamma_{rz} \,\}^T, \tag{26}$$

for a model where the z-axis is the axis of symmetry, and the out-of-plane coordinate is the tangent direction, θ, as shown in Fig. 3.

Finite-element analyses of bamboo

This section discusses the numerical modeling of bamboo under simple load cases in order to illustrate the differences between computed results obtained using different material models. The selected load cases include tension, torsion and bending. Several material models are considered and discussed comparatively.

Model geometry

In geometry, bamboo is essentially a hollow cylinder with periodic stiffeners called diaphragms, located at positions called nodes (see Fig. 7). A bamboo cell is the section of culm between two diaphragms. The diameter of the culm is tapered, being largest near the ground. As illustrated in Fig. 8, the internal and external diameter of the cell modeled in this study are

D_i = 56 mm and D_e = 80 mm, respectively. Cell wall thickness is t = 12 mm, internodal distance is L = 350 mm, and the angle of taper is neglected. Figure 8 illustrates the geometry of the modeled cell. The nodes at locations A, B and C were selected for stress evaluation in the numerical examples. A fillet was created to transition the diaphragm into the cell wall. This simulates actual bamboo structures and eliminates stress concentrations that would be created by the presence of sharp corners. The fillet radius in the present models is 14 mm, which equals 1/4th of the inner diameter of the cell. For the load cases of tension and torsion, one bamboo cell was modeled. For bending, two cells were modeled in order to include one diaphragm in the interior of the domain away from applied loads and support conditions.

Material properties and models

The elastic properties considered in this study employ the Young's moduli obtained by Nogata and Takahashi through detailed experiments [1]. They tested several small specimens cut from different locations through the thickness of the wall of the culm. These tests allowed them to determine the variation of Young's modulus that occurs through the wall thickness due to the graded distribution of longitudinal bamboo fibers. Nogata and Takahashi [1] used the rule of mixtures to estimate a Young's modulus for the fibers of E_f=55 GPa, for the surrounding matrix of E_m=2 GPa, and for the bulk material of E_b=15 GPa. Here, we employ a Poisson's ratio of 0.35 [5]. The estimated variation of Young's modulus through the bamboo thickness is given by the expression [1]

$$E(r) = 3.75e^{(2.2r/t)}, \tag{27}$$

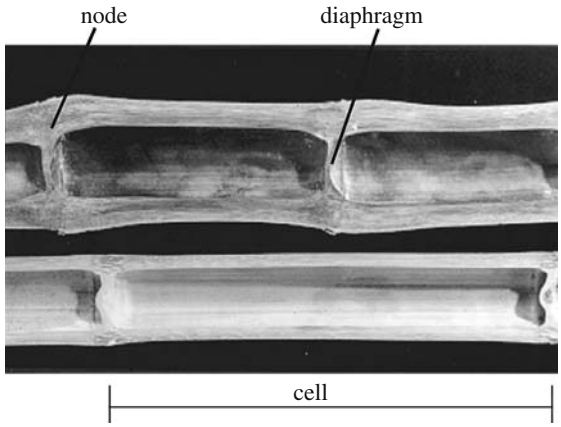

Fig. 7 Cross section of bamboo culm showing internal structure (photo courtesy of [8])

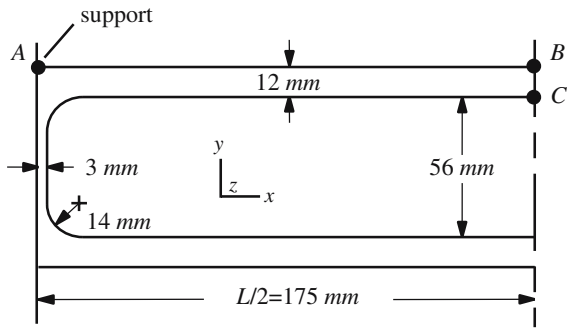

Fig. 8 Section view of one-half of cell showing dimensions adopted for finite-element meshes

where r denotes position through the thickness of the cell wall starting at the inner surface, and t is the thickness of the cell wall. For the exponential material variation expressed by Eq. (27), the axisymmetric stiffness tensor is expressed as

$$\mathbf{E}(r) = \frac{(1-v)E(r)}{(1+v)(1-2v)} \begin{bmatrix} 1 & \frac{v}{1-v} & \frac{v}{1-v} & 0 \\ \frac{v}{1-v} & 1 & \frac{v}{1-v} & 0 \\ \frac{v}{1-v} & \frac{v}{1-v} & 1 & 0 \\ 0 & 0 & 0 & \frac{1-2v}{2(1-v)} \end{bmatrix}. \tag{28}$$

The variation expressed by Eq. (27) corresponds to a common bamboo species known as Moso bamboo, or *Phyllostachys pubescens* Mazel (Gramineae), and was found to vary somewhat between different locations of the same bamboo stalk [1]. For the 12 mm cell wall thickness of the model used in this study, Eq. (27) gives a maximum modulus of 33.84 GPa at the outer edge of the wall.

To study bamboo behavior using different material models, three types of material models were considered for each of the load cases of tension, torsion and bending [35]. The first model considers a homogeneous isotropic structure with a bulk Young's modulus determined from the following expression:

$$E_b = \frac{\int_{r=0}^{r=t} 3.75e^{(2.2r/t)}dr}{t}, \tag{29}$$

which yields E_b=13.68 GPa. This is close to the value of E_b=15.00 GPa for the bulk material reported by Nogata and Takahashi [1], which was presumably obtained through the rule of mixtures. Using the rule of mixtures, E_b = 15.00 GPa would reflect a volume fraction of fibers in the cell wall of approximately 25%, and a matrix volume fraction of approximately 75%.

The second material model considers the continuous gradation of Young's modulus through the thickness of the cell wall as described by Eq. (27). Although bam-

boo cell diaphragms contain fibers, these are neglected in the current study. All material within the inner diameter of D_i = 56 mm is assigned a Young's modulus of E = 3.75 GPa, which corresponds to the modulus at the interior edge of the cell wall, as prescribed by Eq. (27).

Finally, the third material model studied here is a homogeneous orthotropic material whose elastic stiffness matrix is obtained using the homogenization method described in Section 3 with the material variation described by Eq. 27. In this case the effective axisymmetric elasticity tensor obtained through homogenization (see Section 3) considering a 20×20 mesh for the unit cell is

$$\mathbf{E}^H = \begin{bmatrix} E_{rr} & E_{r\theta} & E_{rz} & 0 \\ E_{r\theta} & E_{\theta\theta} & E_{z\theta} & 0 \\ E_{rz} & E_{z\theta} & E_{zz} & 0 \\ 0 & 0 & 0 & E_{rz} \end{bmatrix} = \begin{bmatrix} 14.91 & 8.03 & 8.03 & 0 \\ 8.03 & 21.95 & 9.78 & 0 \\ 8.03 & 9.78 & 19.91 & 0 \\ 0 & 0 & 0 & 3.44 \end{bmatrix} \text{GPa}. \quad (30)$$

These properties will be considered in a homogeneous orthotropic FEM model of the bamboo structure. Cylindrical coordinates represent the most natural orientation in which to perform the analysis of this axisymmetric structure [36].

The objective of comparing these material models is to illustrate differences in displacements and stresses computed by a variety of numerical representations of material gradients. It is also necessary to investigate under what circumstances bamboo can be modeled as a simplified homogeneous structure using averaged or effective properties, and when it may be beneficial or necessary to incorporate material variation in the model to capture actual gradients through the cell wall.

Finite-element meshes and boundary conditions

Figure 9(a) illustrates the mesh discretization in the finite-element model used to simulate tension and torsion loading. The mesh consists of 30 sectors of elements surrounding the axis of symmetry, for a total of 7,380 20-noded, tri-quadratic brick elements. Quadratic elements have been shown to capture the effects of material gradients much more effectively than linear elements [30, 37], and are used here to ensure accurate modeling of the bamboo cell wall. Figure 9(b) shows a detailed view of the mesh near the end/cell diaphragm where support conditions are applied. An axisymmetric model with the same mesh discretization shown in Fig. 9(b) was used to analyze the bamboo modeled as a homogenized orthotropic material. That mesh consisted of 246 8-noded axisymmetric quadrilateral elements and 847 nodes. Integration of order 2 was employed for all analyses ($2 \times 2 \times 2$ integration rule for three-dimensional (3-D) 20-noded brick elements, and 2×2 integration rule for 2-D 8-noded axisymmetric elements). Because the homogenization procedure described in Section 3 of this study applies to axisymmetric models, only tension loading is considered for the homogenized orthotropic material case. A 3-D homogenization procedure analogous to the procedures in Section 3 may be employed to obtain orthotropic material properties for cases such as torsion and bending where loading is not axisymmetric.

A few comments about loading without axial symmetry (such as the torsion and bending cases) are in order. In this situation, the radial, circumferential and axial displacement components are each functions of r, θ and z. Although the problem becomes 3-D, it can be solved by combining the results of multiple 2-D problems (e.g., by representing the loading by components in the form of a trigonometric series) [26, 27]. The advantage of this approach is that full domain discretization in the θ-direction is not required. Commercial software provides for this kind of analysis, however we opted not to address the cases of non-axisymmetric loading.

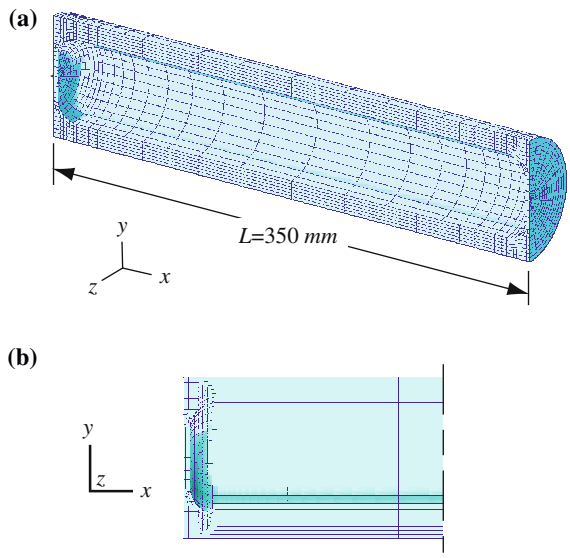

Fig. 9 Bamboo cell mesh discretization: (**a**) FEM model built for tension and torsion loading includes 7,380 20-noded brick finite elements and 33,794 nodes; (**b**) View of mesh discretization at end of cell

For tension loading, displacements of all nodes at one end of the cell model are constrained in the x-direction, and pressure was applied to the faces of some elements on the opposite end. Additional nodal constraints were applied to prevent rigid-body motion. Loaded element faces included the four outer-most rings of elements, lying between D = 58.53 mm and the exterior diameter, D_e = 80 mm. Applied tension is limited to these elements in order to confine loading to the cell walls, thus avoiding artificially loading the diaphragm. A schematic illustrating tension loading of the bamboo cell model is shown in Fig. 10(a).

For torsion loading, all nodes at one end of the cell model are fixed in all directions. Torque is applied to the opposite end through four nodal loads at D_e = 80 mm acting tangent to the surface. Figure 10(b) shows a schematic of the bamboo cell model with torsion boundary conditions. In order to ensure an even distribution of torque from the applied nodal loads to the cell wall, all elements with one face on the end surface of the cell model were assigned a very high Young's modulus.

Figure 11(a) shows a section view of the mesh employed to simulate the bending load case, and Fig. 11(b) shows a detailed view of the mesh in the region of the interior node. A schematic of the boundary conditions for bending is shown in Fig. 12. For this problem, one end of the mesh was fixed, and loads were applied to five nodes at the opposite end of the model to ensure an even loading distribution. Elements connected to the loaded nodes were also assigned a high value of Young's modulus to ensure that the point loads would not lead to excessive local distortions of the mesh.

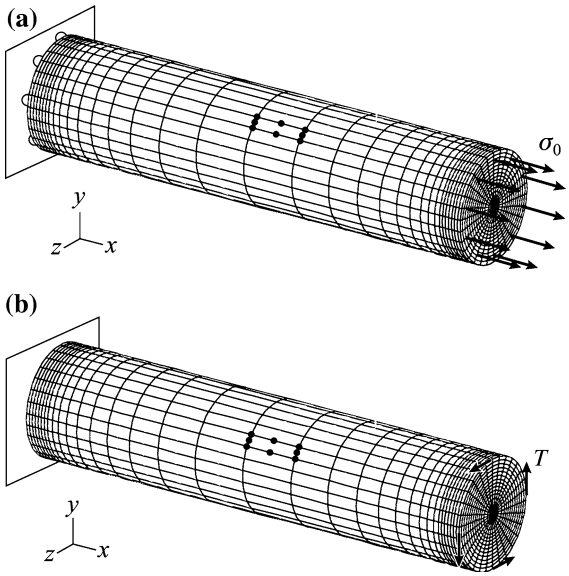

Fig. 10 Schematic of boundary conditions and applied loads for (**a**) tension loading; (**b**) torsion loading

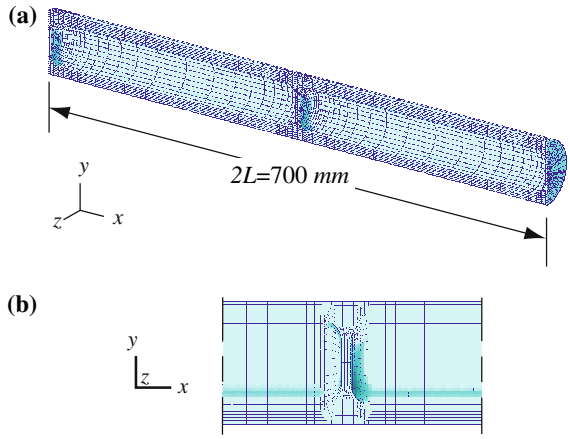

Fig. 11 Bamboo discretization for the bending load case: (**a**) Cross section of two-cell FEM model. Full mesh includes 14,760 20-noded brick finite elements and 66,417 nodes; (**b**) Detail of mesh at interior bamboo node region

Numerical results

This section provides sample numerical results from the analyzed load cases. Table 1 lists the maximum displacement that occurs at the loaded end of each specimen. With reference to the coordinate system shown in Figs. 10 and 12, displacement for tension is in the $+x$-direction, for bending is in the $-y$-direction, and for torsion is the angle of rotation. Values are normalized by the maximum theoretical displacements/rotation of a hollow cylinder having the same diameter, length and wall thickness as the bamboo cell. The hollow cylinder of reference is assumed to have material properties E=13.68 GPa and ν=0.35, and is acted upon by the same axial force, bending load and torque that displace the finite-element models. The normalized expressions are

$$(u_{\text{tens}})_n = \frac{u_{\text{tens}}}{PL/(AE)}, \quad (v_{\text{bend}})_n = \frac{v_{\text{bend}}}{\frac{FL^3}{3EI}\left(1+\frac{3f_sEI}{GAL^2}\right)}, \quad (\phi_{\text{tors}})_n = \frac{\phi_{\text{tors}}}{TL/(GI_p)}, \tag{31}$$

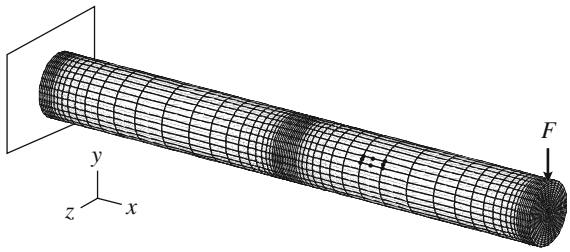

Fig. 12 Schematic of boundary conditions and applied load for bending case

Table 1 Displacements at loaded end of models, normalized by corresponding displacements in a homogeneous hollow cylinder with properties E = 13.68 GPa and ν = 0.35

Material properties	Normalized maximum displacement at loaded end		
	$(u_{\text{tens}})_n$	$(\phi_{\text{tors}})_n$	$(v_{\text{bend}})_n$
Homogeneous E=13.68 GPa ν=0.35	0.996	0.988	0.999
FGM $E(r)=3.75e^{(2.2r/t)}$ ν =0.35	0.978	0.836	0.845
Orthotropic $\mathbf{E}^H$ (homogenized) (see Eq. (30))	0.868	–	–

where subscript n denotes normalized values, u_{tens} is the axial displacement for tension, v_{bend} is the vertical displacement for bending, and ϕ_{tors} is the angle of rotation for torsion loading. The denominator of each expression in Eq. (31) is the theoretical expression for displacement [38], where P is the total axial load, A is the cross-sectional area of the hollow cylinder, L is the cylinder length, and E is the homogeneous Young's modulus. The theoretical expression for the tip displacement of a cantilever beam includes the contributions of bending and shear. Force F is the total applied load, G is the homogeneous shear modulus ($E/[2(1+\nu)]$), and f_s is the shape factor for shear. The value of f_s = 2 employed here corresponds to a thin hollow cylinder [38]. In the rotation expression for torque, I_p is the polar moment of inertia of the hollow cylinder.

Table 1 shows that in all cases, the model that incorporates material variation through the thickness of the cell wall is stiffer than the model that employs a homogeneous Young's modulus obtained from averaging the expression for material variation in Eq. (27). If the Young's modulus of 15 GPa estimated by Nogata and Takahashi [1] for the bulk material had been employed in the simulations, the deformation behavior of the homogeneous model and the FGM model would be even more similar. The axisymmetric model based on homogenized orthotropic material is the stiffest of the three cases. The close agreement between axial deformations in the FGM and homogeneous isotropic model indicates that the use of averaged (or bulk) properties is consistent for estimating elongation. The homogenized orthotropic material model leads to displacements that differ from the other two models, thus indicating that the presented homogenization procedure, based on the assumptions of Section 3, affects the axial stiffness of the cell wall. Further adjustments would be required in the model to ensure that computed axial deformation corresponds to the other models. For torsion and bending loading, comparison between the FGM and homogeneous material models indicates that the homogeneous approximation leads to a more flexible structure. This is expected because the FGM model places the stiffest material farthest away from the neutral axis. Figures 13–15 show fringe plots of total-deformation magnitude in the models under tension, torsion and bending loads, respectively. Deformation values in these plots are normalized by the maximum displacement found in any of the models in each figure. Figures 13(a)–(b) illustrate the similarity between the FGM and averaged homogeneous material models under tension.

Table 2 lists computed stress values at three locations in the bamboo cell, indicated by points A, B and C in Fig. 8. Values are normalized by the corresponding theoretical stresses of a hollow cylinder having the same diameter, length and wall thickness as the bamboo cell [38]. Again, the hollow cylinder is assumed to have material properties E = 13.68 GPa and ν = 0.35, and is acted upon by the same axial force, bending load and torque that displace the finite-element models. Normalization of stresses follows

$$(\sigma_{xx\_\text{tens}})_n = \frac{\sigma_{xx\_\text{tens}}}{P/A}, \quad (\tau_{xz\_\text{tors}})_n = \frac{\tau_{xz\_\text{tors}}}{Tr/I_p}, \quad (\sigma_{xx\_\text{bend}})_n = \frac{\sigma_{xx\_\text{bend}}}{My/I}, \tag{32}$$

where σ_{xx_tens} is the axial stress due to axial load P, τ_{xz_bend} is the shear stress due to torque T, and σ_{xx_bend}

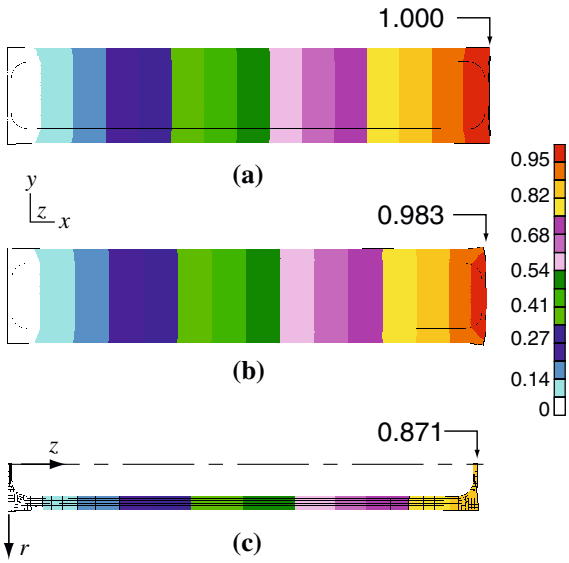

Fig. 13 Fringe plots of total-deformation magnitude for tension loading of (**a**) homogeneous isotropic, (**b**) FGM, and (**c**) homogeneous orthotropic models. Deformations are normalized by the maximum displacement that occurs among the three models

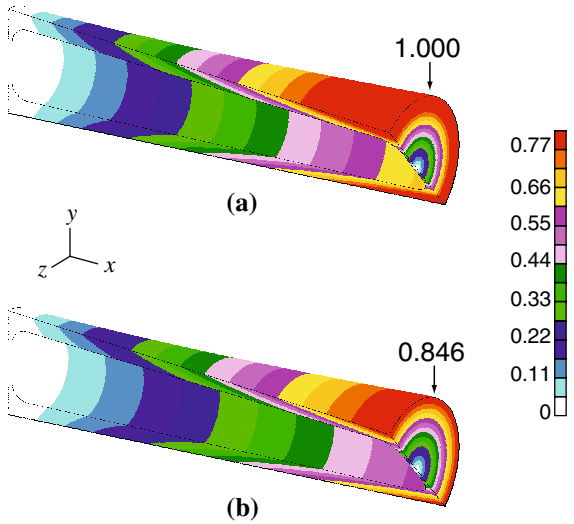

Fig. 14 Fringe plots of total-deformation magnitude for torsion loading of (**a**) homogeneous isotropic and (**b**) FGM models. Deformations are normalized by the maximum displacement that occurs among the two models

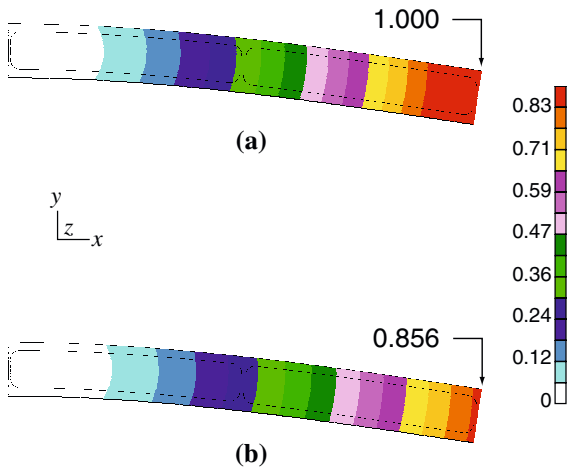

Fig. 15 Total-deformation magnitude for models under bending. (**a**) Homogeneous isotropic material; (**b**) FGM. Deformations are normalized by the maximum displacement that occurs among the two models

is the bending stress due to the applied moment $M=F \times 2L$.

Table 2 illustrates the effect of material gradients on stresses in the bamboo cell wall. Stresses near the interior of the wall are much lower in the actual material as represented by the FGM, than they are in the homogeneous case. Stresses near the outside of the cell wall are much higher in the FGM case than in the homogeneous case. Thus, the FGM leads to a remarkable stress redistribution in the bamboo and the stress response of (inhomogeneous) FGMs differs substantially from those of their homogeneous counterparts (c.f. [30]). Figures 16–18 show fringe plots of the von Mises stress in the models under tension, torsion and bending loads, respectively. Stress values in these plots are normalized by the maximum stress found in any of the models in each figure. For each loading condition, the highest stresses appear near support boundary conditions or applied nodal loads. The plots demonstrate that material gradients through the cell wall have a strong influence on local cell-wall stresses. The model that employs homogenized orthotropic material, shown in Fig. 16(c), leads to nearly identical stresses in the mid-section of the cell as the homogeneous isotropic material model shown in Fig. 16(a).

Conclusions and extensions

Numerical simulations of bamboo structure using finite element method and a multiscale method were performed. By using the graded finite element concept the continuous change of bamboo properties along the thickness could be taken into account, and its influence in the bamboo mechanical behavior was shown. By using the homogenization method for graded material, the effective properties of an axisymmetric bamboo composite were computed. By means of these homogenized properties it is possible to model bamboo as a homogeneous orthotropic medium. However, further

Table 2 Stresses at locations indicated by *A*, *B* and *C* in Fig. 8. Stresses are normalized by the stresses at location *A* in a homogeneous hollow cylinder with properties E = 13.68 GPa and ν = 0.35

Material properties	Location (see Fig. 8)	Normalized stress		
		$(\sigma_{xx\_\text{tens}})_n$	$(\tau_{xz\_\text{tors}})_n$	$(\sigma_{xx\_\text{bend}})_n$
homogeneous E=13.68 GPa ν =0.35	*A*	1.17	0.888	2.50
	B	1.00	1.00	1.00
	C	1.00	0.702	0.703
FGM $E(r)=3.75e^{(2.2r/t)}$ ν =0.35	*A*	2.45	2.00	4.47
	B	2.31	2.08	2.08
	C	0.255	0.160	0.160
Orthotropic $\mathbf{E}^H$ (homogenized) (see Eq. (30))	*A*	1.14	–	–
	B	1.00	–	–
	C	1.00	—	—

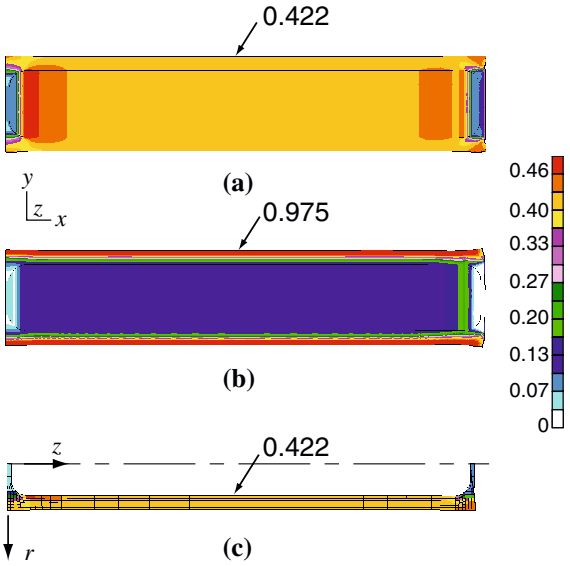

Fig. 16 Fringe plots of von Mises stress distribution for tension case. (**a**) Homogeneous isotropic, (**b**) FGM, and (**c**) homogeneous orthotropic material. Stresses are normalized by the maximum stress value that occurs among the three models

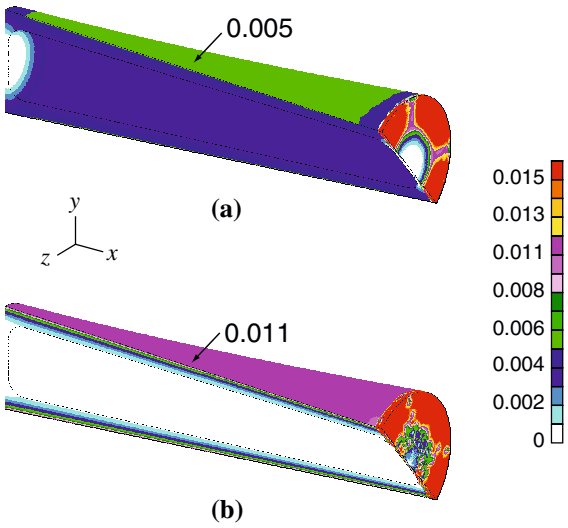

Fig. 17 Von Mises stress distributions for torsion loading. (**a**) Homogeneous isotropic; (**b**) FGM model. Stresses are normalized by the maximum stress value that occurs among the two models

research is needed to link theoretical descriptions provided by functions such as the hypothetical one in Eq. (22), with actual bamboo properties. This link may be established through integrated investigations involving experiments and observed behavior of bamboo structures.

Given the additional computational effort of the homogenization procedure, it seems that a simple averaged elastic modulus obtained from a rule of mixtures or an averaged modulus obtained from the FGM

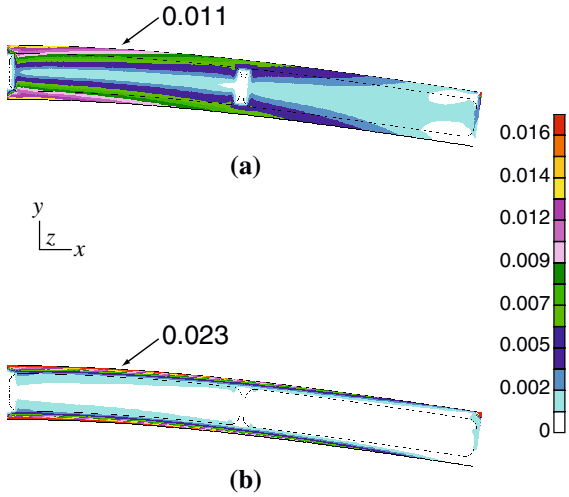

Fig. 18 Von Mises stress distributions for bending. (**a**) Homogeneous isotropic; (**b**) FGM material. Stresses are normalized by the maximum stress value that occurs among the two models

variation will provide suitable numerical accuracy for capturing the ''global'' deflection/response of a bamboo structure. To estimate local features, however, such as stresses near supports, pin connections or holes etc., it is necessary to employ a numerical procedure that accurately models material gradients through the cell wall. In this study, the use of graded elements to model the FGM structure of bamboo captures the much higher stresses that exist near the exterior of the bamboo wall due to the higher stiffness of that fiber-dense region and also the stress redistribution through the bamboo wall. These wall stresses will be magnified by holes or by the bearing loads imposed at connections. This work illustrates modern numerical analysis techniques that lend special insight into the structural and mechanical response of bamboo as a naturally graded fiber composite.

Acknowledgements We gratefully acknowledge the U.S. National Science Foundation through the project CMS #0303492 ''Inter-Americas Collaboration in Materials Research and Education'' (P.I., Professor W. Soboyejo, Princeton University).

References

1. Nogata F, Takahashi H (1995) Compos Eng 5:743
2. Janssen JJA (1995) Building with bamboo. Intermediate Technology Publications, London
3. Jayanetti DL, Follett PR (1998) Bamboo in construction. Trada, UK
4. Chung KF, Yu WK (2002) Eng Struct 24:429
5. Ghavami K (1995) Cement Concrete Compos 17:281
6. Okubo K, Fujii T, Yamamoto Y (2004) Compos Part A 35:377
7. Ge XC, Li XH, Meng YZ (2004) J Appl Polymer Sci 93:1804
8. Ghavami K (2004) Structure and Properties of Bamboo. PowerPoint presentation

9. Amada S, Munekata T, Nagase Y, Ichikawa Y, Kirigai A, Yang ZF (1996) J Compos Mat 30:800
10. Amada S, Ichikawa Y, Munekata T, Shimizu H (1997) Compos Part B 28:13
11. Ray AK, Das SK, Mondal S, Ramachandrarao P (2004) J Mater Sci 39:1055
12. Amada S, Ichikawa Y, Munekata T, Nagase Y, Shimizu H (1997) Compos Part B 28:13
13. Ghavami K, Rodrigues CS, Paciornik S (2003) Asian J Civil Eng 4:1
14. Janssen JJA (1991) Mechanical properties of bamboo. Kluwer Academic Publishers
15. Suresh S, Mortensen A (1988) Fundamentals of functionally graded materials. IOM Communications, London
16. Paulino GH, Jin Z-H, Dodds RH Jr (2003) In: Karihaloo B, Knauss WG (eds) Comprehensive structural integrity, vol 2. Elsevier, p 607
17. Lakkad SC, Patel JM (1980) Fibre Sci Tech 14:319
18. Lo TY, Cui HZ, Leung HC (2004) Mater Lett 58:2595
19. Li SH, Zeng QY, Xiao YL, Fu SY, Zhou BL (1995) Mat Sci Eng C 3:125
20. Amada S, Lakes RS (1997) J Mater Sci 32:2693
21. Amada S, Untao S (2001) Compos Part B 32:451
22. Nugroho N, Ando N (2001) J Wood Sci 47:237
23. Lee AWC, Bai XS, Bangi AP (1997) Forest Prod J 47:74
24. Amada S, Terauchi Y (2001) In: Trumble K, Bowman K, Reimanis I, Sampath S (eds) Proceedings of the 6th International Symposium of Functionally Graded Materials, Estes Park, Colorado, Sep. 2000. The American Ceramic Society, p 763
25. Bai XS, Lee AWC, Thompson LL, Rosowsky DV (1999) Wood Fiber Sci 31:403
26. Bathe K-J (1996) Finite element procedures. Prentice-Hall, Englewood Cliffs
27. Cook RD, Malkus DS, Plesha ME, Witt RJ (2002) Concepts and applications of finite element analysis 4th edn. John Wiley and Sons, USA
28. Sanchez-Palencia E (1980) Non-homogeneous media and vibration. Theory lecture notes in physics 127. Springer, Berlin
29. Santare MH, Lambros J (2000) ASME J Appl Mech 67:819
30. Kim J-H, Paulino GH (2002) ASME J Appl Mech 69:502
31. Yin HM, Sun LZ, Paulino GH (2004) Acta Mater 52:3535
32. Nemat-Nasser S, Hori M (1993) Micromechanics: overall properties of heterogeneous materials. North-Holland, Amsterdam
33. Kalamkarov AL, Kolpakov AG (1997) Analysis, design and optimization of composite structures. John Wiley and Sons, Chichester, England
34. Guedes JM, Kikuchi N (1990) Comp Meth Appl Mech Eng 83:143
35. Rooney F, Ferrari M (2001) Int J Solids Struct 38:413
36. Pindera MJ, Freed AD, Arnold SM (1993) Int J Solids Struct 30:1213
37. Walters MC, Paulino GH, Dodds RH Jr (2004) Int J Solids Struct 41:1081
38. Gere JM, Timoshenko SP (1990) Mechanics of Materials 3rd edn. PWS Publishing, Boston